Precise Finite-Element Model for Pulleys Based on the Hamiltonian Form of Elasticity

Xiangjun Qiu[1]; Chang Chai[2]; and Ryan Lemmon[3]

Abstract: Conveyor pulleys are typical axisymmetric structures subjected to nonaxisymmetric loading. Taking full advantage of the characteristics of the pulley structure, this paper presents a precise finite-element formulation for pulley stress analysis based on the Hamiltonian form of elasticity. In the model, the solution is expanded into a set of Fourier series; a paired set of state variables are selected from the Fourier coefficients; and the governing equations are reorganized in Hamiltonian form with the use of the paired state variables. The general solutions to the Hamiltonian system can be obtained numerically and formulated into a finite-element model, from which the final stress solution for a pulley can be found. Numerical examples show that this method is much more efficient than the conventional FEM with comparable accuracy.
DOI: 10.1061/(ASCE)EM.1943-7889.0000746.

Author keywords: Pulley; Fourier series; Hamiltonian system; Precise finite-element method (FEM); Timoshenko beam; Shell and plate.

Introduction

A conveyor pulley consists of rim, disk, and shaft components assembled through weld and locking devices (Fig. 1). In a belt conveyor system, pulleys play important roles as drive pulley, tail pulley, take-up pulley, and bend pulley. In a typical, long-distance conveyor system, where the belt tension can be as high as several million Newtons, a pulley is subjected to severe bending and torsional load. Failure of a pulley in a conveyor system may be catastrophic. Therefore, accurate and efficient modeling of stress distribution in a pulley is of significant scientific and engineering value. The effort of modeling stress distribution in a pulley structure can be traced to the 1960s, when Lange (1963) tried to use an approximate analytical method to estimate the conveyor pulley stress. But modern FEM results have proven that Lange's work was very inaccurate (Qiu and Sethi 1993).

Currently, according to Patel et al. (2011), the most popular method used for pulley stress analysis is the FEM. Ravikumar and Chattopadhyay (1999) developed a two-dimensional (2D) finite-element model based on Fourier series for pulley stress analysis. Martins and Kovesdy (2012) summarized the use of three-dimensional (3D) solid elements to solve the conveyor pulley stress problem. Many people reported the use of commercial FEM software to compute the pulley stress distributions (Sethi and Nordell 1993; Pathan et al. 2011). As computer hardware technology advances, the computational time for completion of a FEM analysis of a conveyor pulley is shortened from a few days in the 1990s to less than 1 h today.

Still, designers never stop seeking more efficient methods for pulley stress analysis for the purpose of efficient design optimization among various options. Qiu and Sethi (1993) developed a very efficient and effective analytical model for pulley stress distribution named modified transfer matrix method (MTMM). It uses the paired displacement-stress variables to reorganize the governing equations, expresses the general solution in the form of transfer matrix, and further modifies the transfer matrix form into a finite-element formulation. But this method relies on the availability of the analytical solution of the governing equation for each pulley component. In case the governing equations are too complicated to obtain an analytical solution, an approximate solution has to be used as a substitute. In Qiu and Sethi's (1993) work, the major approximate solution employed was Timoshenko and Woinowsky-Krieger's (1959) approximate solution to the cylindrical shell, in which the terms of circumferential displacement in strain-displacement relations are neglected for mathematical convenience. The consequence of this approximation is that four of six modes of rigid body motions are no longer preserved in the solution and errors are unavoidable in certain cases.

This paper modifies the Qiu and Sethi (1993) model by (1) presenting the governing equations for each pulley component in a form of Hamiltonian system without any approximation, (2) deriving the general solution to the Hamiltonian system using a precise numerical integration method, (3) reorganizing the general solution in finite-element form, and (4) numerically solving the finite-element equations for final stress solution. This modification leads to a new method named precise FEM (PFEM). It must be pointed out that the fundamental ideas of PFEM are similar to those used in Qiu's (2006, 2009) boundary element models for rolling resistance. The interrelation of the model presented in this paper to the rolling resistance models (Qiu 2006, 2009) is addressed subsequently.

Governing Equations, Hamiltonian Systems, and PFEM

Fig. 1 shows a pulley structure, which, from the mechanics point of view, consists of cylindrical shell, plate, and beam components. The theories of shell, plate, and beam are used to develop a precise finite element for each component.

[1]Chief Scientist, High Fidelity Simulation, Metso Minerals, 4820 Centennial Blvd., Colorado Springs, CO 80919. E-mail: Xiangjun.Qiu@metso.com

[2]Associate Professor, School of Machinery and Automobile Engineering, Hefei Univ. of Technology, Hefei, Anhui 230009, China (corresponding author). E-mail: chai416@163.com

[3]President, Advanced Conveyor Technologies Inc., 3911 E. 132 N, Rigby, ID 83442. E-mail: lemmon@actek.com

Note. This manuscript was submitted on February 14, 2013; approved on October 30, 2013; published online on November 4, 2013. Discussion period open until July 11, 2014; separate discussions must be submitted for individual papers. This paper is part of the ***Journal of Engineering Mechanics***, © ASCE, ISSN 0733-9399/04014057(12)/$25.00.

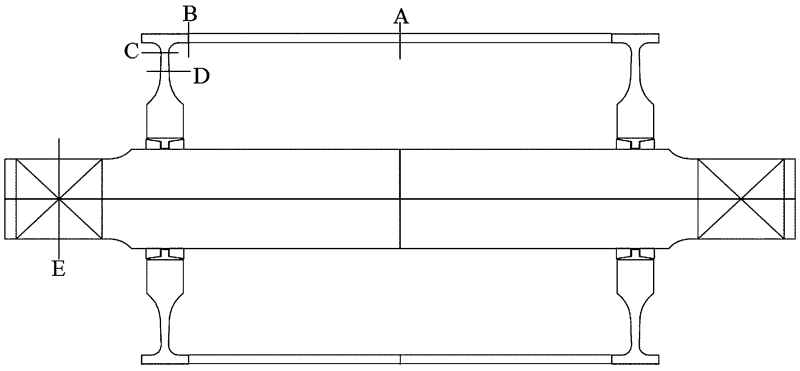

Fig. 1. Profile of a pulley structure

Modeling Rim as Thin-Walled Cylindrical Shell

Fig. 2 shows the coordinate system for a cylindrical shell with radius R and the stresses and stress couples acting on a differential element. According to Ventsel and Krauthammer (2001), the equilibrium equations can be written as

$$\frac{\partial N_1}{\partial x}+\frac{1}{R}\frac{\partial N_{21}}{\partial \theta}+X=0 \tag{1}$$

$$\frac{\partial N_{12}}{\partial x}+\frac{1}{R}\frac{\partial N_2}{\partial \theta}+\frac{Q_2}{R}+Y=0 \tag{2}$$

$$\frac{\partial Q_1}{\partial x}+\frac{1}{R}\frac{\partial Q_2}{\partial \theta}-\frac{N_2}{R}+Z=0 \tag{3}$$

$$Q_1=\frac{\partial M_1}{\partial x}+\frac{1}{R}\frac{\partial M_{21}}{\partial \theta} \tag{4}$$

$$Q_2=\frac{\partial M_{12}}{\partial x}+\frac{1}{R}\frac{\partial M_2}{\partial \theta} \tag{5}$$

$$N_{12}-N_{21}-\frac{M_{21}}{R}=0 \tag{6}$$

where N_1, N_2, N_{21}, and N_{12} = membrane stresses; Q_1 and Q_2 = transverse stresses; and M_1, M_2, M_{12}, and M_{21} = stress couples (see Fig. 2 for the positive senses of these stresses and stress couples); X, Y, and Z = components of external surface load in x-, q-, and z-directions, respectively; the constitutive equations can be written as

$$N_1=\frac{Et}{1-\mu^2}\left(\frac{\partial u}{\partial x}+\mu\frac{1}{R}\frac{\partial v}{\partial \theta}+\mu\frac{w}{R}\right) \tag{7}$$

$$N_2=\frac{Et}{1-\mu^2}\left(\frac{1}{R}\frac{\partial v}{\partial \theta}+\frac{w}{R}+\mu\frac{\partial u}{\partial x}\right) \tag{8}$$

$$N_{21}=\frac{Et}{2(1+\mu)}\left(\frac{1}{R}\frac{\partial u}{\partial \theta}+\frac{\partial v}{\partial x}\right) \tag{9}$$

$$M_1=-D\left(\frac{\partial^2 w}{\partial x^2}+\mu\frac{1}{R^2}\frac{\partial^2 w}{\partial \theta^2}-\mu\frac{1}{R^2}\frac{\partial v}{\partial \theta}\right) \tag{10}$$

$$M_2=-D\left(\frac{1}{R^2}\frac{\partial^2 w}{\partial \theta^2}-\frac{1}{R^2}\frac{\partial v}{\partial \theta}+\mu\frac{\partial^2 w}{\partial x^2}\right) \tag{11}$$

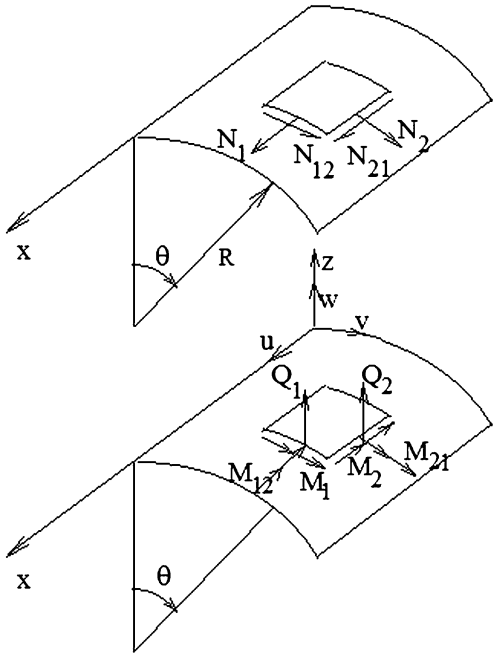

Fig. 2. Stresses on rim cylindrical differential element

$$M_{12}=M_{21}=-D(1-\mu)\left(\frac{1}{R}\frac{\partial^2 w}{\partial x\partial \theta}-\frac{1}{R}\frac{\partial v}{\partial x}\right) \tag{12}$$

where u, v, and w = displacements in x-, θ-, and z-directions, respectively; E and μ = Young's modulus and Poisson's ratio of the pulley material; and $D=Et^3/12(1-\mu^2)$. The boundary conditions on the edge $x=x^*$ can be formulated in terms of the following four pairs of displacement-stress variables:

$$(u, v, w, \varphi, N_1, F_1, V_1, M_1) \tag{13}$$

where

$$F_1=N_{21}+2\frac{M_{12}}{R} \tag{14}$$

$$V_1 = \frac{\partial M_1}{\partial x} + \frac{2}{R}\frac{\partial M_{12}}{\partial \theta} \tag{15}$$

$$\varphi = -\frac{\partial w}{\partial x} \tag{16}$$

Eliminating Q_1, Q_2, M_{21}, and N_{12}, from Eqs. (1)–(6) and Eqs. (13)–(15), the equilibrium equations can be reduced to the following:

$$\frac{\partial N_1}{\partial x} + \frac{1}{R}\frac{\partial N_{21}}{\partial \theta} + X = 0 \tag{17}$$

$$\frac{\partial F_1}{\partial x} + \frac{1}{R}\frac{\partial N_2}{\partial \theta} + \frac{1}{R^2}\frac{\partial M_2}{\partial \theta} + Y = 0 \tag{18}$$

$$\frac{\partial V_1}{\partial x} + \frac{1}{R^2}\frac{\partial^2 M_2}{\partial \theta^2} - \frac{N_2}{R} + Z = 0 \tag{19}$$

Because of axisymmetry, the solution can be expressed by the following Fourier series:

$$u(x,\theta) = u_0(x) + \sum_{n=1}^{\infty}[u_n(x)\cos n\theta + u_{-n}(x)\sin n\theta] \tag{20}$$

$$v(x,\theta) = v_0(x) + \sum_{n=1}^{\infty}[v_n(x)\sin n\theta + v_{-n}(x)\cos n\theta] \tag{21}$$

$$w(x,\theta) = w_0(x) + \sum_{n=1}^{\infty}[w_n(x)\cos n\theta + w_{-n}(x)\sin n\theta] \tag{22}$$

$$N_1(x,\theta) = N_{1,0}(x) + \sum_{n=1}^{\infty}\left[N_{1,n}(x)\cos n\theta + N_{1,-n}(x)\sin n\theta\right] \tag{23}$$

$$N_2(x,\theta) = N_{2,0}(x) + \sum_{n=1}^{\infty}\left[N_{2,n}(x)\cos n\theta + N_{2,-n}(x)\sin n\theta\right] \tag{24}$$

$$N_{21}(x,\theta) = N_{21,0}(x) + \sum_{n=1}^{\infty}\left[N_{21,n}(x)\sin n\theta + N_{21,-n}(x)\cos n\theta\right] \tag{25}$$

$$M_1(x,\theta) = M_{1,0}(x) + \sum_{n=1}^{\infty}\left[M_{1,n}(x)\cos n\theta + M_{1,-n}(x)\sin n\theta\right] \tag{26}$$

$$M_2(x,\theta) = M_{2,0}(x) + \sum_{n=1}^{\infty}\left[M_{2,n}(x)\cos n\theta + M_{2,-n}(x)\sin n\theta\right] \tag{27}$$

$$M_{12}(x,\theta) = M_{12,0}(x) + \sum_{n=1}^{\infty}\left[M_{12,n}(x)\sin n\theta + M_{12,-n}(x)\cos n\theta\right] \tag{28}$$

$$V_1(x,\theta) = V_{1,0}(x) + \sum_{n=1}^{\infty}\left[V_{1,n}(x)\cos n\theta + V_{1,-n}(x)\sin n\theta\right] \tag{29}$$

$$F_1(x,\theta) = F_{1,0}(x) + \sum_{n=1}^{\infty}\left[F_{1,n}(x)\sin n\theta + F_{1,-n}(x)\cos n\theta\right] \tag{30}$$

$$\varphi(x,\theta) = \varphi_0(x) + \sum_{n=1}^{\infty}[\varphi_n(x)\cos n\theta + \varphi_{-n}(x)\sin n\theta] \tag{31}$$

For simplicity, drop the (x) in all the preceding Fourier coefficients [e.g., $N_{1,n}$ stands for $N_{1,n}(x)$].

Substituting Eqs. (20)–(31) into Eqs. (7)–(19)

$$\dot{N}_{1,n} + \frac{n}{R}N_{21} + X_n = 0 \tag{32}$$

$$-\frac{n}{R}N_{2,n} + \dot{F}_{1,n} - \frac{n}{R^2}M_{2,n} + Y_n = 0 \tag{33}$$

$$-\frac{n^2}{R^2}M_{2,n} + \dot{V}_{1,n} - \frac{1}{R}N_{2,n} + Z_n = 0 \tag{34}$$

$$V_{1,n} = \dot{M}_{1,n} + 2\frac{n}{R}M_{12,n} \tag{35}$$

$$F_{1,n} = N_{21,n} + \frac{2}{R}M_{12,n} \tag{36}$$

$$\dot{w}_n = -\varphi_n \tag{37}$$

$$N_{1,n} = \frac{Et}{1-\mu^2}\left(\dot{u}_n + \frac{\mu n}{R}v_n + \frac{\mu}{R}w_n\right) \tag{38}$$

$$N_{2,n} = \frac{Et}{1-\mu^2}\left(\frac{n}{R}v_n + \frac{1}{R}w_n + \mu\dot{u}_n\right) \tag{39}$$

$$N_{21,n} = \frac{Et}{2(1+\mu)}\left(-\frac{n}{R}u_n + \dot{v}_n\right) \tag{40}$$

$$M_{1,n} = D\left(\dot{\varphi}_n + \frac{\mu n^2}{R^2}w_n + \frac{\mu n}{R^2}v_n\right) \tag{41}$$

$$M_{2,n} = D\left(\frac{n^2}{R^2}w_n + \frac{n}{R^2}v_n + \mu\dot{\varphi}_n\right) \tag{42}$$

$$M_{12,n} = -D(1-\mu)\left(\frac{n}{R^2}\varphi_n - \frac{1}{R}\dot{v}_n\right) \tag{43}$$

where the updot symbol denotes the derivative with respect to x (i.e., $\dot{u}_n = du_n/dx$); X_n, Y_n, and Z_n = Fourier coefficients of X, Y, and Z, respectively.

Let

$$q_n = (u_n, v_n, w_n, \varphi_n)^T \quad \text{and}$$
$$p_n = \left(2\pi RN_{1,n},\ 2\pi RF_{1,n},\ 2\pi RV_{1,n},\ 2\pi RM_{1,n}\right)^T \tag{44}$$

From the preceding equations, one can derive the following ordinary differential equation (ODE) for the nth-order Fourier coefficients of q and p of Eq. (44)

$$\begin{Bmatrix}\dot{q}_n\\ \dot{p}_n\end{Bmatrix} = \begin{bmatrix}A_n & B_n\\ C_n & D_n\end{bmatrix}\begin{Bmatrix}q_n\\ p_n\end{Bmatrix} + \begin{Bmatrix}0\\ f_n\end{Bmatrix} \tag{45}$$

where

$$f_n = (-2\pi RX_n, -2\pi RY_n, -2\pi RZ_n, 0)^T \tag{46}$$

$$A_n = \begin{bmatrix} 0 & -\frac{\mu n}{R} & -\frac{\mu}{R} & 0 \\ \frac{EtnR}{EtR^2 + 4(1-\mu^2)D} & 0 & 0 & \frac{4(1-\mu^2)nD}{EtR^2 + 4(1-\mu^2)D} \\ 0 & 0 & 0 & -1 \\ 0 & -\frac{\mu n}{R^2} & -\frac{\mu n^2}{R^2} & 0 \end{bmatrix} \quad (47)$$

$$B_n = \begin{bmatrix} \frac{1-\mu^2}{2\pi REt} & 0 & 0 & 0 \\ 0 & \frac{(1+\mu)R}{\pi EtR^2 + 4\pi(1-\mu^2)D} & 0 & 0 \\ 0 & 0 & 0 & 0 \\ 0 & 0 & 0 & \frac{1}{2\pi RD} \end{bmatrix} \quad (48)$$

$$C_n = \begin{bmatrix} \frac{4\pi(1-\mu)n^2EtD}{EtR^3 + 4(1-\mu^2)RD} & 0 & 0 & -\frac{4\pi(1-\mu)n^2EtD}{EtR^2 + 4(1-\mu^2)D} \\ 0 & \frac{2\pi n^2 Et}{R} + \frac{2\pi(1-\mu^2)n^2D}{R^3} & \frac{2\pi nEt}{R} + \frac{2\pi(1-\mu^2)n^3D}{R^3} & 0 \\ 0 & \frac{2\pi nEt}{R} + \frac{2\pi(1-\mu^2)n^3D}{R^3} & \frac{2\pi Et}{R} + \frac{2\pi(1-\mu^2)n^4D}{R^3} & 0 \\ -\frac{4\pi(1-\mu)n^2EtD}{EtR^2 + 4(1-\mu^2)D} & 0 & 0 & \frac{4\pi n^2(1-\mu)D}{R} - \frac{16\pi(1+\mu)(1-\mu^2)n^2D^2}{EtR^3 + 4(1-\mu^2)RD} \end{bmatrix} \quad (49)$$

$$D_n = \begin{bmatrix} 0 & -\frac{EtnR}{EtR^2 + 4(1-\mu^2)D} & 0 & 0 \\ \frac{\mu n}{R} & 0 & 0 & \frac{\mu n}{R^2} \\ \frac{\mu}{R} & 0 & 0 & \frac{\mu n^2}{R^2} \\ 0 & -\frac{4(1-\mu^2)nD}{EtR^2 + 4(1-\mu^2)D} & 1 & 0 \end{bmatrix} \quad (50)$$

It can be seen that A_n, B_n, C_n, and D_n have the following properties:

$$A_n = -D_n^T; \quad B_n = B_n^T; \quad C_n = C_n^T \quad (51)$$

The general solution to Eq. (45) can be written as

$$\begin{Bmatrix} q_n(x) \\ p_n(x) \end{Bmatrix} = T_n(x) \begin{Bmatrix} q_n(0) \\ p_n(0) \end{Bmatrix} + \int_0^x T_n(x-\tau) \begin{Bmatrix} 0 \\ f_n(\tau) \end{Bmatrix} d\tau \quad (52)$$

where $T_n(x) =$ transfer matrix. Let

$$T_n(x) = \begin{bmatrix} T_{n,qq} & T_{n,qp} \\ T_{n,pq} & T_{n,pp} \end{bmatrix} \quad \text{and} \quad \int_0^x T_n(x-\tau) \begin{Bmatrix} 0 \\ f_n(\tau) \end{Bmatrix} d\tau = \begin{Bmatrix} F_{n,q} \\ F_{n,p} \end{Bmatrix} \quad (53)$$

Eq. (52) can be reorganized in a form of finite-element model

$$K_n U_n = F_{n,\text{int}} + F_{n,\text{ext}} \quad (54)$$

where

$$K_n = \begin{bmatrix} -T_{n,qp} & 0 \\ -T_{n,pp} & -I \end{bmatrix}^{-1} \begin{bmatrix} -T_{n,qq} & I \\ -T_{n,pq} & 0 \end{bmatrix}; \quad U_n = \begin{Bmatrix} q_n(0) \\ q_n(x) \end{Bmatrix};$$

$$F_{n,\text{int}} = \begin{Bmatrix} -p_n(0) \\ p_n(x) \end{Bmatrix}; \quad \text{and} \quad F_{n,\text{ext}} = \begin{bmatrix} -T_{n,qp} & 0 \\ -T_{n,pp} & -I \end{bmatrix}^{-1} \begin{Bmatrix} F_{n,q} \\ F_{n,p} \end{Bmatrix}$$

The following comments apply to these preceding equations:

1. The mathematical properties described by Eq. (51) guarantee that the ODEs of Eq. (45) are a Hamiltonian system (Vinogradov and Kupershmidt 1981; Zhong 1995). The corresponding Hamiltonian function can be expressed as $H(p_n, q_n) = 1/2 p_n^T B_n p_n + p_n^T A_n q_n - 1/2 q_n^T C_n q_n$. With the use of Hamiltonian function, Eq. (45) also can be written as $\dot{q}_n = \partial H/\partial p_n$ and $\dot{p}_n = -(\partial H/\partial q_n)$
   Note that the mathematical properties of Eq. (51) only can be preserved when the displacement-stress pairs of variables, called state variables, for boundary conditions [i.e., Eq. (13)] are selected correctly.
2. It is difficult to obtain the transfer matrix $T_n(x)$ of Eq. (52) analytically. But $T_n(x)$ can be calculated precisely by using the so-called precise numerical integration method suggested by Zhong et al. (1996).
3. Because Eq. (54) takes the form of a finite-element model, it can be assembled with other finite elements discussed subsequently to form a global FEM equation to represent the mechanical behavior of a pulley structure. Because there is no interpolation approximation used in the development of Eq. (54) [i.e., the formulation of Eq. (54) is mathematically exact], the authors call the precise finite-element model developed in this paper the PFEM.

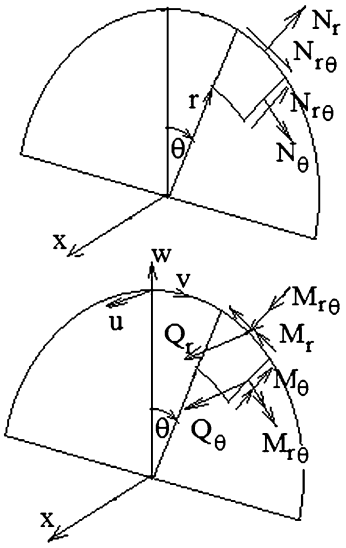

Fig. 3. Stresses on disk plate differential element

4. It is noted that in Qiu's (2006, 2009) boundary element models for rolling resistance, a similar form of governing ODE to that of Eq. (45) is derived, which can be proved to satisfy the properties of Eq. (51) in the domain of complex numbers.
5. In Qiu and Sethi (1993), the terms associated with the circumferential displacement v in Eqs. (10)–(12) are omitted for the purpose of convenience to obtain analytical solution of transfer matrix (Timoshenko and Woinowsky-Krieger 1959). The consequence of the omission is that four modes of rigid body motions are no longer preserved.

Modeling Disk as Thin-Walled Circular Plate

Fig. 3 shows the coordinate system for a circular plate and the stresses and stress couples acting on a differential element. The thickness, denoted by t, of the circular plate varies as the following function of radius:

$$t = cr^b \tag{55}$$

According to Ventsel and Krauthammer (2001), the equilibrium equations can be written as

$$\frac{\partial N_r}{\partial r} + \frac{N_r - N_\theta}{r} + \frac{1}{r}\frac{\partial N_{r\theta}}{\partial \theta} = 0 \tag{56}$$

$$\frac{\partial N_{r\theta}}{\partial r} + 2\frac{\partial N_{r\theta}}{r} + \frac{1}{r}\frac{\partial N_\theta}{\partial \theta} = 0 \tag{57}$$

$$\frac{\partial Q_r}{\partial r} + \frac{Q_r}{r} - \frac{1}{r}\frac{\partial Q_\theta}{\partial \theta} = 0 \tag{58}$$

$$Q_r = \frac{\partial M_r}{\partial r} + \frac{M_r - M_\theta}{r} - \frac{1}{r}\frac{\partial M_{r\theta}}{\partial \theta} \tag{59}$$

$$Q_\theta = \frac{\partial M_{r\theta}}{\partial r} + 2\frac{M_{r\theta}}{r} - \frac{1}{r}\frac{\partial M_\theta}{\partial \theta} \tag{60}$$

where N_r, N_θ, and $N_{r\theta}$ = membrane stresses; Q_r and Q_θ = transverse stresses; and M_r, M_θ, and $M_{r\theta}$ = stress couples (see Fig. 3 for the positive senses of these stresses and stress couples); the constitutive equations can be written as

$$N_r = \frac{Et}{1-\mu^2}\left(\frac{\partial w}{\partial r} + \mu\frac{1}{r}\frac{\partial v}{\partial \theta} + \mu\frac{w}{r}\right) \tag{61}$$

$$N_\theta = \frac{Et}{1-\mu^2}\left(\frac{1}{r}\frac{\partial v}{\partial \theta} + \frac{w}{r} + \mu\frac{\partial w}{\partial r}\right) \tag{62}$$

$$N_{r\theta} = \frac{Et}{2(1+\mu)}\left(\frac{1}{r}\frac{\partial w}{\partial \theta} + \frac{\partial v}{\partial r} - \frac{v}{r}\right) \tag{63}$$

$$M_r = -D\left(\frac{\partial^2 u}{\partial r^2} + \mu\frac{1}{r^2}\frac{\partial^2 u}{\partial \theta^2} + \mu\frac{1}{r}\frac{\partial u}{\partial r}\right) \tag{64}$$

$$M_\theta = -D\left(\frac{1}{r^2}\frac{\partial^2 u}{\partial \theta^2} + \frac{1}{r}\frac{\partial u}{\partial r} + \mu\frac{\partial^2 u}{\partial r^2}\right) \tag{65}$$

$$M_{r\theta} = D(1-\mu)\left(\frac{1}{r}\frac{\partial^2 u}{\partial r \partial \theta} - \frac{1}{r^2}\frac{\partial u}{\partial \theta}\right) \tag{66}$$

where u, v, and w = displacements in x-, θ-, and r-directions, respectively; and the boundary conditions on the edge $r = r^*$ can be formulated in terms of the following four pairs of displacement-stress variables:

$$(u, v, w, \varphi, V_r, N_{r\theta}, N_r, -M_r) \tag{67}$$

where

$$\varphi = \frac{\partial u}{\partial r} \tag{68}$$

$$V_r = Q_r - \frac{1}{r}\frac{\partial M_{r\theta}}{\partial \theta} \tag{69}$$

Eliminating Q_r and Q_θ from Eqs. (57)–(59) and Eq. (68)

$$\frac{\partial V_r}{\partial r} + \frac{V_r}{r} - \frac{2}{r^2}\frac{\partial M_{r\theta}}{\partial \theta} + \frac{1}{r^2}\frac{\partial^2 M_\theta}{\partial \theta^2} = 0 \tag{70}$$

$$V_r = \frac{\partial M_r}{\partial r} + \frac{M_r - M_\theta}{r} - \frac{2}{r}\frac{\partial M_{r\theta}}{\partial \theta} \tag{71}$$

Because of axisymmetry, the solution can be expressed by the following Fourier series:

$$u(r,\theta) = u_0(r) + \sum_{n=1}^{\infty}[u_n(r)\cos n\theta + u_{-n}(r)\sin n\theta] \tag{72}$$

$$v(r,\theta) = v_0(r) + \sum_{n=1}^{\infty}[v_n(r)\sin n\theta + v_{-n}(r)\cos n\theta] \tag{73}$$

$$w(r,\theta) = w_0(r) + \sum_{n=1}^{\infty}[w_n(r)\cos n\theta + w_{-n}(r)\sin n\theta] \tag{74}$$

$$N_r(r,\theta) = N_{r,0}(r) + \sum_{n=1}^{\infty}\left[N_{r,n}(r)\cos n\theta + N_{r,-n}(r)\sin n\theta\right] \tag{75}$$

$$N_\theta(r,\theta) = N_{\theta,0}(r) + \sum_{n=1}^{\infty}\left[N_{\theta,n}(r)\cos n\theta + N_{\theta,-n}(r)\sin n\theta\right] \quad (76)$$

$$N_{r\theta}(r,\theta) = N_{r\theta,0}(r) + \sum_{n=1}^{\infty}\left[N_{r\theta,n}(r)\sin n\theta + N_{r\theta,-n}(r)\cos n\theta\right] \quad (77)$$

$$M_r(r,\theta) = M_{r,0}(r) + \sum_{n=1}^{\infty}\left[M_{r,n}(r)\cos n\theta + M_{r,-n}(r)\sin n\theta\right] \quad (78)$$

$$M_\theta(r,\theta) = M_{\theta,0}(r) + \sum_{n=1}^{\infty}\left[M_{\theta,n}(r)\cos n\theta + M_{\theta,-n}(r)\sin n\theta\right] \quad (79)$$

$$M_{r\theta}(r,\theta) = M_{r\theta,0}(r) + \sum_{n=1}^{\infty}\left[M_{r\theta,n}(r)\sin n\theta + M_{r\theta,-n}(r)\cos n\theta\right] \quad (80)$$

$$V_r(r,\theta) = V_{r,0}(r) + \sum_{n=1}^{\infty}\left[V_{r,n}(r)\cos n\theta + V_{r,-n}(r)\sin n\theta\right] \quad (81)$$

$$\varphi(r,\theta) = \varphi_0(r) + \sum_{n=1}^{\infty}\left[\varphi_n(r)\cos n\theta + \varphi_{-n}(r)\sin n\theta\right] \quad (82)$$

For simplicity, drop the (r) in all the preceding Fourier coefficients. Substituting Eqs. (72)–(82) into Eqs. (56) and (57), Eqs. (61)–(68), and Eqs. (70) and (71), and denoting the derivative with respect to r by the up dot symbol (i.e., $\dot{u}_n = du_n/dr$)

$$r\dot{N}_{r,n} + N_{r,n} - N_{\theta,n} + nN_{r\theta,n} = 0 \quad (83)$$

$$r\dot{N}_{r\theta,n} + 2N_{r\theta,n} - nN_{\theta,n} = 0 \quad (84)$$

$$r\dot{V}_{r,n} + V_{r,n} - \frac{2n}{r}M_{r\theta,n} - \frac{n^2}{r}M_{\theta,n} = 0 \quad (85)$$

$$rV_{r,n} = r\dot{M}_{r,n} + M_{r,n} - M_{\theta,n} - 2nM_{r\theta,n} \quad (86)$$

$$\dot{u}_n = \varphi_n \quad (87)$$

$$N_{r,n} = \frac{Et}{1-\mu^2}\left(\dot{w}_n + \frac{\mu}{r}w_n + \frac{\mu n}{r}v_n\right) \quad (88)$$

$$N_{\theta,n} = \frac{Et}{1-\mu^2}\left(\frac{1}{r}w_n + \frac{n}{r}v_n + \mu\dot{w}_n\right) \quad (89)$$

$$N_{r\theta,n} = \frac{Et}{2+\mu}\left(\dot{v}_n - \frac{n}{r}w_n - \frac{1}{r}v_n\right) \quad (90)$$

$$M_{r,n} = -D\left(\dot{\varphi}_n + \frac{\mu}{r}\dot{u}_n - \frac{\mu n^2}{r^2}u_n\right) \quad (91)$$

$$M_{\theta,n} = -D\left(\frac{1}{r}\dot{u}_n - \frac{n^2}{r^2}u_n + \mu\dot{\varphi}_n\right) \quad (92)$$

$$M_{r\theta,n} = D(1-\mu)\left(-\frac{n}{r}\varphi_n + \frac{n}{r^2}u_n\right) \quad (93)$$

Let

$$q_n = (u_n, v_n, w_n, \varphi_n)^T \quad \text{and}$$
$$p_n = \left(2\pi r V_{r,n},\, 2\pi r N_{r\theta,n},\, 2\pi r N_{r,n}, -2\pi r M_{r,n}\right)^T \quad (94)$$

From the preceding equations, one can derive the following ODE for the nth-order Fourier coefficients of q and p of Eq. (94)

$$\begin{Bmatrix}\dot{q}_n\\ \dot{p}_n\end{Bmatrix} = \begin{bmatrix}A_n & B_n\\ C_n & D_n\end{bmatrix}\begin{Bmatrix}q_n\\ p_n\end{Bmatrix} \quad (95)$$

where

$$A_n = \begin{bmatrix}0 & 0 & 0 & 1\\ 0 & 1/r & n/r & 0\\ 0 & -\mu n/r & -\mu/r & 0\\ \mu n^2/r^2 & 0 & 0 & -\mu/r\end{bmatrix} \quad (96)$$

$$B_n = \begin{bmatrix}0 & 0 & 0 & 0\\ 0 & \frac{1+\mu}{\pi r Et} & 0 & 0\\ 0 & 0 & \frac{1-\mu^2}{2\pi r Et} & 0\\ 0 & 0 & 0 & \frac{1}{2\pi r D}\end{bmatrix} \quad (97)$$

$$C_n = \begin{bmatrix}\frac{2\pi(2-2\mu+n^2-\mu^2n^2)n^2D}{r^3} & 0 & 0 & \frac{2\pi(\mu^2+2\mu-3)n^2D}{r^2}\\ 0 & \frac{2\pi n^2 Et}{r} & \frac{2\pi n Et}{r} & 0\\ 0 & \frac{2\pi n Et}{r} & \frac{2\pi Et}{r} & 0\\ \frac{2\pi(\mu^2+2\mu-3)n^2D}{r^2} & 0 & 0 & \frac{2\pi(1-\mu^2+2n^2-2n^2\mu)D}{r}\end{bmatrix} \quad (98)$$

$$D_n = \begin{bmatrix} 0 & 0 & 0 & -\mu n^2/r^2 \\ 0 & -1/r & n\mu/r & 0 \\ 0 & -n/r & \mu/r & 0 \\ -1 & 0 & 0 & \mu/r \end{bmatrix} \tag{99}$$

It can be seen that A_n, B_n, C_n, and D_n satisfy the properties of a linear Hamiltonian system described by Eq. (51). The general solution to Eq. (95) can be written as

$$\begin{Bmatrix} q_n(r) \\ p_n(r) \end{Bmatrix} = T_n(r, r_0) \begin{Bmatrix} q_n(r_0) \\ p_n(r_0) \end{Bmatrix} \tag{100}$$

where $T_n(r, r_0)$ = transfer matrix. Let

$$T_n(r, r_0) = \begin{bmatrix} T_{n,qq} & T_{n,qp} \\ T_{n,pq} & T_{n,pp} \end{bmatrix} \tag{101}$$

Following the same procedure of development of Eq. (54), one can rewrite Eq. (100) in a form of finite-element model

$$K_n U_n = F_n \tag{102}$$

where

$$K_n = \begin{bmatrix} -T_{n,qp} & 0 \\ -T_{n,pp} & -I \end{bmatrix}^{-1} \begin{bmatrix} -T_{n,qq} & I \\ -T_{n,pq} & 0 \end{bmatrix}; \quad U_n = \begin{Bmatrix} q_n(r_0) \\ q_n(r) \end{Bmatrix};$$

$$\text{and} \quad F_n = \begin{Bmatrix} -p_n(r_0) \\ p_n(r) \end{Bmatrix}$$

To obtain accurate numerical solution of $T_n(r, r_0)$, make the following transformation

$$q_n = S_q(r) q_n^* \quad \text{and} \quad p_n = S_p(r) p_n^* \tag{103}$$

where

$$q_n^* = (u_n, v_n, w_n, r\varphi_n)^T$$

$$p_n^* = \left(2\pi r^{3-3b} V_{r,n}, 2\pi r^{1-b} N_{r\theta,n}, 2\pi r^{1-b} N_{r,n}, -2\pi r^{2-3b} M_{r,n}\right)^T$$

$$S_q(r) = \text{diag}[\,1 \quad 1 \quad 1 \quad 1/r\,]$$

$$S_p(r) = \text{diag}\left[r^{-2+3b} \quad r^b \quad r^b \quad r^{-1+3b}\right]$$

where diag[...] = diagonal matrix; and b = parameter defined in Eq. (55). Substituting Eq. (103) into Eq. (95), one obtains a new set of ODEs with constant coefficients

$$\frac{d}{d\ln r} \begin{Bmatrix} q_n^* \\ p_n^* \end{Bmatrix} = \begin{bmatrix} \tilde{A}_n & \tilde{B}_n \\ \tilde{C}_n & \tilde{D}_n \end{bmatrix} \begin{Bmatrix} q_n^* \\ p_n^* \end{Bmatrix} \tag{104}$$

where

$$\tilde{A}_n = \begin{bmatrix} 0 & 0 & 0 & 1 \\ 0 & 1 & n & 0 \\ 0 & -\mu n & -\mu & 0 \\ \mu n^2 & 0 & 0 & 1-\mu \end{bmatrix} \tag{105}$$

$$\tilde{B}_n = \begin{bmatrix} 0 & 0 & 0 & 0 \\ 0 & \dfrac{1+\mu}{\pi E c} & 0 & 0 \\ 0 & 0 & \dfrac{1-\mu^2}{2\pi E c} & 0 \\ 0 & 0 & 0 & \dfrac{6(1-\mu^2)}{\pi E c^3} \end{bmatrix} \tag{106}$$

$$\tilde{C}_n = \begin{bmatrix} \dfrac{2\pi(2-2\mu+n^2-\mu^2 n^2) n^2 E c^3}{12(1-\mu^2)} & 0 & 0 & \dfrac{2\pi(\mu^2+2\mu-3) n^2 E c^3}{12(1-\mu^2)} \\ 0 & 2\pi n^2 E c & 2\pi n E c & 0 \\ 0 & 2\pi n E c & 2\pi E c & 0 \\ \dfrac{2\pi(\mu^2+2\mu-3) n^2 E c^3}{12(1-\mu^2)} & 0 & 0 & \dfrac{2\pi(1-\mu^2+2n^2-2n^2\mu) E c^3}{12(1-\mu^2)} \end{bmatrix} \tag{107}$$

$$\tilde{D}_n = \begin{bmatrix} 2-3b & 0 & 0 & -\mu n^2 \\ 0 & -1-b & n\mu & 0 \\ 0 & -n & \mu-b & 0 \\ -1 & 0 & 0 & 1+\mu-3b \end{bmatrix} \tag{108}$$

where c is defined in Eq. (55). For Eq. (104), one can obtain accurate numerical solution $T_n^*(\ln r - \ln r_0)$ and then use Eq. (103) to find the solution

$$T_n(r, r_0) = \begin{bmatrix} S_q(r) & 0 \\ 0 & S_p(r) \end{bmatrix} T_n^*(\ln r - \ln r_0) \begin{bmatrix} S_q(r_0) & 0 \\ 0 & S_p(r_0) \end{bmatrix}^{-1} \tag{109}$$

Modeling Shaft as Beam and Bar

The pulley shaft is treated as a beam for bending and a bar for tension and torsion (Fig. 4). As proved by Qiu and Sethi (1993), the following mathematically exact beam element can be obtained by use of Timoshenko's beam theory:

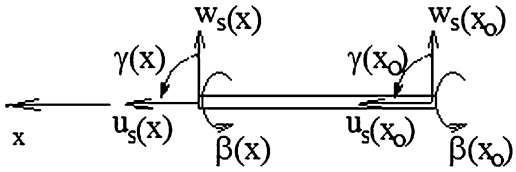

Fig. 4. Beam element for shaft

$$K_{bm}U_{bm} = F_{bm} \tag{110}$$

where

$$U_{bm} = (w_{s0}, \gamma_0, w_{sx}, \gamma_x)^T$$
$$F_{bm} = (V_0, M_0, V_x, M_x)^T$$
$$K_{bm} = \begin{bmatrix} \frac{12EI_s}{L^3(1+\alpha)} & \frac{6EI_s}{L^2(1+\alpha)} & -\frac{12EI_s}{L^3(1+\alpha)} & \frac{6EI_s}{L^2(1+\alpha)} \\ \frac{6EI_s}{L^2(1+\alpha)} & \frac{(4+\alpha)EI_s}{L(1+\alpha)} & -\frac{6EI_s}{L^2(1+\alpha)} & \frac{12EI_s}{L^3(1+\alpha)} \\ -\frac{12EI_s}{L^3(1+\alpha)} & -\frac{6EI_s}{L^2(1+\alpha)} & \frac{12EI_s}{L^3(1+\alpha)} & -\frac{6EI_s}{L^2(1+\alpha)} \\ \frac{6EI_s}{L^2(1+\alpha)} & \frac{(2-\alpha)EI_s}{L(1+\alpha)} & -\frac{6EI_s}{L^2(1+\alpha)} & \frac{(4+\alpha)EI_s}{L(1+\alpha)} \end{bmatrix} \tag{111}$$

where $w_{s0} = w_s(x_0)$, $w_{sx} = w_s(x)$, $\gamma_0 = \gamma(x_0)$, $\gamma_x = \gamma(x)$; $w_s(x)$ and $\gamma(x)$ = transverse displacement and rotation angle of the beam axis, respectively; $V(x)$ and $M(x)$ = transverse force and moment acting at the cross section of the beam; I_s = area moment of inertia; $L = x - x_0$; and $\alpha = 12EI_s/(L^2kaG)$ where k is a shape factor equal to 0.75 for circular cross section, a is the area of the cross section, and G is the shear modulus.

For tension and torsion loading, the following mathematically exact element applies:

$$K_{\text{bar}}U_{\text{bar}} = F_{\text{bar}} \tag{112}$$

where

$$U_{\text{bar}} = (u_{s0}, \beta_0, u_{sx}, \beta_x)^T$$
$$F_{\text{bar}} = (N_0, M_{t0}, N_x, M_{tx})^T$$
$$K_{\text{bar}} = \begin{bmatrix} \frac{EA}{L} & 0 & -\frac{EA}{L} & 0 \\ 0 & \frac{GJ_s}{L} & 0 & -\frac{GJ_s}{L} \\ -\frac{EA}{L} & 0 & \frac{EA}{L} & 0 \\ 0 & -\frac{GJ_s}{L} & 0 & \frac{GJ_s}{L} \end{bmatrix} \tag{113}$$

where $u_{s0} = u_s(x_0)$, $u_{sx} = u_s(x)$, $\beta_0 = \beta(x_0)$, $\beta_x = \beta(x)$; $u_s(x)$ and $\beta(x)$ = axial displacement and rotational angle about axis of the shaft, respectively; $N(x)$ and $M_t(x)$ = tension and torsional moment acting at the cross section, respectively; and J_s = polar moment of inertia.

Assembly of Global Finite Elements

Fig. 5 shows a division of finite elements for a pulley. The assembly method of the precise finite elements discussed previously is the same as that in conventional FEM. Special attention, however, must be paid to the connection between the shaft element and the disk element. In beam and bar theories, a major assumption is that plane sections remain plane. According to this assumption, the shaft beam element only can contribute to the Fourier series term of $n = 1$ and -1; and the shaft bar element only can contribute to the Fourier series term of $n = 0$. Therefore, at the point of connection between the shaft and disk, the following conditions are imposed to connect the shaft with the disk:

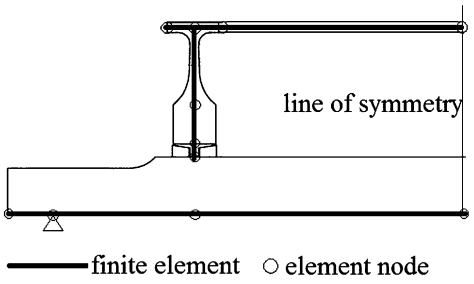

Fig. 5. Finite-element divisions for a pulley

$$w_n = -nv_n \quad n = -1, 1 \tag{114}$$

$$u_n = R_{\text{shaft}}\varphi_n \quad n = -1, 1 \tag{115}$$

$$w_s = w_n \quad n = -1, 1 \tag{116}$$

$$\gamma = \varphi_n \quad n = -1, 1 \tag{117}$$

$$u_s = u_n \quad n = 0 \tag{118}$$

$$\beta = v_n/R_{\text{shaft}} \quad n = 0 \tag{119}$$

$$u_n = v_n = w_n = 0, \quad \varphi_n = 0 \quad |n| > 1 \tag{120}$$

where R_{shaft} = radius of the shaft at the connection point.

The belt tension applies a pressure and shear stress on the surface of the pulley rim. Fig. 6. shows a typical distribution of such a loading. The pressure and shear stress, as a periodic function of θ, can be expanded into Fourier series. The coefficients of the pressure and shear stress are the terms of Z_n and Y_n in Eq. (46). Due to the nature of loading, $X_n = 0$ in Eq. (46). The integration term of Eq. (52) can be evaluated by using any of the numerical integration methods, of which 5 points Gauss quadrature is recommended.

Examples

Two examples are given to demonstrate the validity of PFEM for pulley stress analysis. One is a bend pulley and the other is a drive pulley. The major parameters for both pulleys are listed in Table 1. In the two examples, the pulleys (Fig. 1) are analyzed by using both PFEM and *ANSYS 10* FEM. Owing to symmetry, only half of the pulley is modeled.

FEM Model

In the *ANSYS* FEM model for pulley, two types of axisymmetric-harmonic structural solid elements [Plan 25 (four nodes per element)

and Plan 83 (eight nodes per element)] and two types of meshes [coarse mesh (1,088 elements) and fine mesh (4,690 elements)] are tested for convergence. There are 71 ($-36 < n < 36$) Fourier terms used in the FEM model. Fig. 7 shows the distribution of stress component σ_x. From Fig. 7, it is observed that there is a tendency for solutions to converge to the solution of the Plan 83 model with fine mesh as the mesh gets finer and/or the order of element's polynomial (interpolation) function gets higher. Other stress components not shown in Fig. 7 have similar trends to that of σ_x. Further calculations indicate the following:

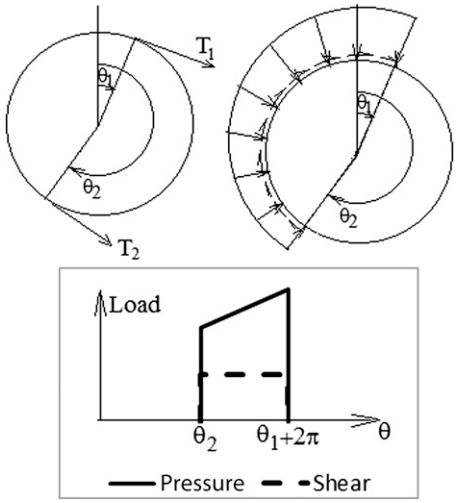

Fig. 6. Loading on pulley surface

Table 1. Model Parameters

Parameters	Case 1: bend pulley	Case 2: drive pulley
Material properties		
E (GPa)	206.9	206.9
μ	0.3	0.3
Rim geometry		
Length (mm)	1,550	2,200
Diameter (mm)	610	1,362
Thickness (mm)	20	38
Belt width (mm)	1,300	2,000
Disk geometry		
Locking device width (mm)	88	141
Hub outer diameter (mm)	380	800
Hub inner diameter (mm)	250	515
Hub width (mm)	117	155
Disk parameter, c	381	4,189
Disk parameter, b	−0.433	−0.760
Shaft geometry		
Diameter (mm)	190	420
Length (mm)	2,240	3,360
Bearing-bearing distance (mm)	1,950	2,900
Disk-disk distance (mm)	1,280	2,000
Loading parameters		
$\theta 1$ (degrees)	−10	0
$\theta 2$ (degrees)	270	180
$T1$ (kN)	197	1,018
$T2$ (kN)	196	633

1. The deviations of the stress solutions of Plan 25 model with coarse and fine meshes with respect to the solution of Plan 83 model with fine mesh are around 17 and 12%, respectively, in terms of RMS error defined as

$$\text{RMS\_ER}(\sigma) = \frac{\sqrt{\frac{\sum_{i=1}^{N}\left(\sigma_i^{\text{Test}} - \sigma_i^{\text{P83Fine}}\right)^2}{N}}}{\|\sigma\|_\infty} \tag{121}$$

2. The deviation of the stress solutions of Plan 83 model with coarse mesh with respect to that of Plan 83 model with fine meshes is around 1% in terms of RMS error.

Using the preceding deviation numbers and FEM h-p convergence criterion, the authors concluded that the *ANSYS* Plan 83 element model with fine mesh yields a sufficient accurate solution for pulley stresses. Therefore, *ANSYS* Plan 83 element model with fine meshes (3,662 and 4,690 elements for the bend and drive pulleys, respectively) was chosen to calculate stresses for the bend and drive pulleys specified in Table 1, respectively, for the purpose of validation and verification of PFEM.

Validation and Verification of PFEM

In a PFEM model, only 20 elements are employed; there are 71 ($-36 < n < 36$) Fourier terms used in a PFEM model.

Figs. 8–15 demonstrate the results of stress distributions at locations A, B, C, and D obtained by the PFEM and *ANSYS*. To quantitatively estimate the numerical deviation between the results

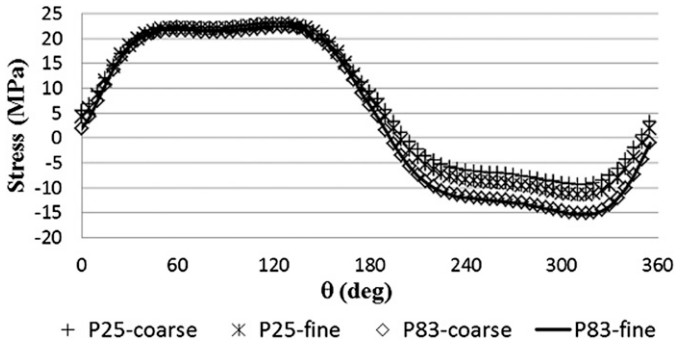

Fig. 7. Observation of convergence of stress σ_x calculated by *ANSYS* for Case 2, at location B inside of rim

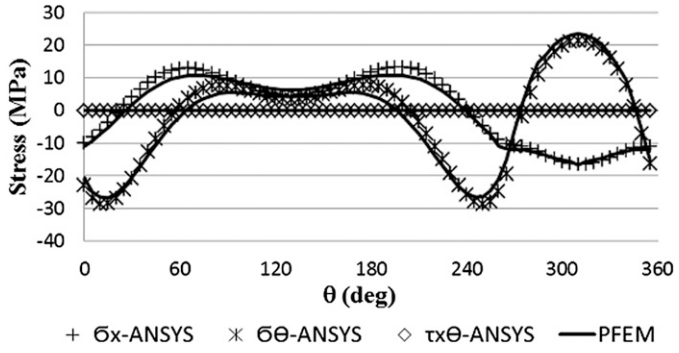

Fig. 8. Case 1, at location A inside of rim, $RE(\sigma_x) = 9.3\%$, $RE(\sigma_\theta) = 8.2\%$

of PFEM and *ANSYS*, the following RMS error function, denoted as $RE(\sigma)$, was used first to measure the relative deviation:

$$RE(\sigma) = \frac{\sqrt{\frac{\sum_{i=1}^{N}\left(\sigma_i^{\text{PFEM}} - \sigma_i^{ANSYS}\right)^2}{N}}}{\|\sigma\|_\infty} \tag{122}$$

Figs. 8–15 contain the $RE(\sigma)$ numbers for each stress component. Secondly, Tables 2 and 3 give a direct comparison of principal stresses calculated by PFEM to those calculated by *ANSYS* at locations where extreme values (denoted $\sigma_{1\max}$ and $\sigma_{2\min}$) occurred.

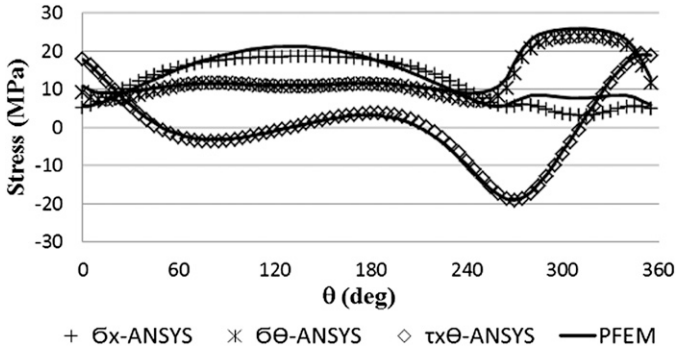

Fig. 9. Case 1, at location B inside of rim, $RE(\sigma_x) = 11.9\%$, $RE(\sigma_\theta) = 5.8\%$, $RE(\tau_{x\theta}) = 3.0\%$

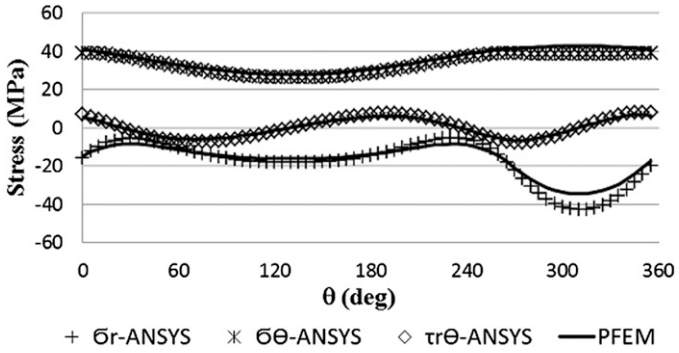

Fig. 10. Case 1, at location C inside of plate, $RE(\sigma_r) = 8.1\%$, $RE(\sigma_\theta) = 5.7\%$, $RE(\tau_{r\theta}) = 6.8\%$

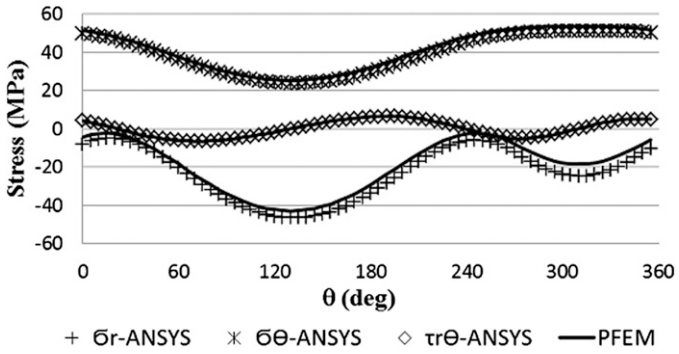

Fig. 11. Case 1, at location D inside of plate, $RE(\sigma_r) = 8.9\%$, $RE(\sigma_\theta) = 4.1\%$, $RE(\tau_{r\theta}) = 4.0\%$

Evident in Figs. 8–15 and Tables 2 and 3, at locations A and D the up bond of *RE* values are within 9–10% and the up bond of errors of $\sigma_{1\max}$ and $\sigma_{2\min}$ are within 10%; while at locations B and C the up bond of *RE* values are within 12–17% and the up bond of errors of $\sigma_{1\max}$ and $\sigma_{2\min}$ are within 16–19%. The larger discrepancies of stresses of PFEM from those of *ANSYS* at locations B and C may be owing to the fact that locations B and C are much closer to the joint region between the rim and the disk, where the 3D stress state cannot be accurately modeled by the 2D shell and plate theories. However, the inaccuracies of stress distributions in locations B and C are within 16–19% and, therefore, are within the engineering allowable margin.

The PFEM computation for each pulley only takes less than a second to finish on a laptop computer with a 1.8-GHz AMD processor. *ANSYS* computations take approximately 14 and 34 min, respectively, for the bend and drive pulleys on a desktop computer with a 3.07-GHz Inter Core i7–950 processor. Also, it is worth noting that one of the strengths of PFEM is the much easier set-up of the model and analysis by using only the information from Table 1. On the other hand, the full FEM model of the pulley, which can handle precisely the pulley geometry and yield accurate solution at locations of stress concentrations, requires a lot of manual preparation work, such as mesh adjustment and test of solution convergence. Thus, the authors suggest a way to combine the strengths of both PFEM and FEM in the pulley design process: use of PFEM for preliminary optimization (i.e., selection of good candidate designs among hundreds of candidates) and use of FEM for the final optimization (i.e., selection of the best design among a few good candidates).

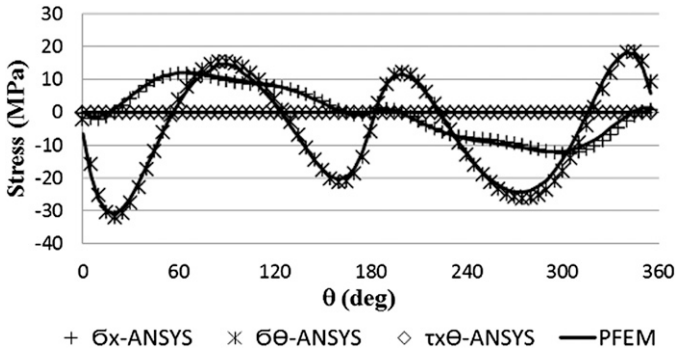

Fig. 12. Case 2, at location A inside of rim, $RE(\sigma_x) = 3.9\%$, $RE(\sigma_\theta) = 5.3\%$

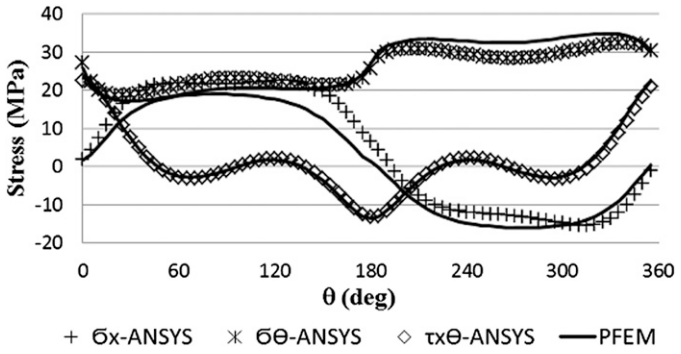

Fig. 13. Case 2, at location B inside of rim, $RE(\sigma_x) = 17.1\%$, $RE(\sigma_\theta) = 8.2\%$, $RE(\tau_{x\theta}) = 4.8\%$

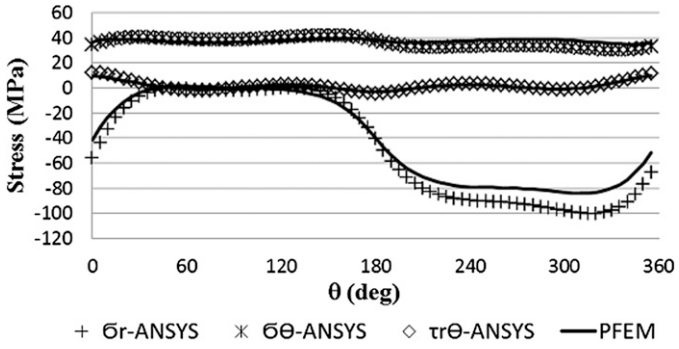

Fig. 14. Case 2, at location C inside of plate, $RE(\sigma_r) = 9.6\%$, $RE(\sigma_\theta) = 8.4\%$, $RE(\tau_{r\theta}) = 7.9\%$

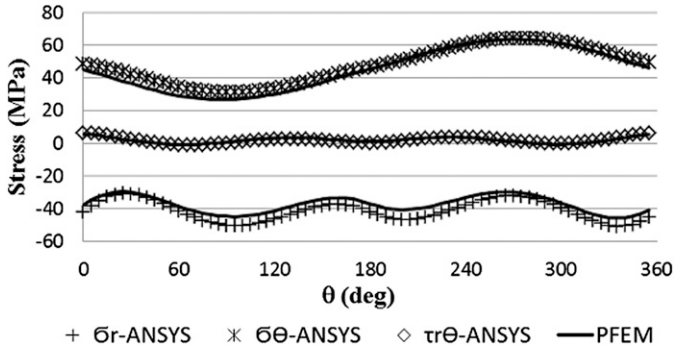

Fig. 15. Case 2, at location D inside of plate, $RE(\sigma_r) = 8.7\%$, $RE(\sigma_\theta) = 7.1\%$, $RE(\tau_{r\theta}) = 5.6\%$

Table 2. Case 1 Extreme Stresses (MPa) and Bearing Reaction Force (kN) by PFEM

Location	Stress type	θ (degrees)	*ANSYS*	PFEM	Error (%)
Cross section A inner	σ_{1max}	310	21.5	23.5	9.6
surface	σ_{2min}	250	−28.7	−26.4	8.0
Cross section B inner	σ_{1max}	345	32.0	33.9	5.8
surface	σ_{2min}	0	−11.0	−9.9	9.8
Cross section C inner	σ_{1max}	355	40.1	41.8	4.2
surface	σ_{2min}	310	−43.0	−34.7	19.2
Cross section D inner	σ_{1max}	340	51.4	53.4	4.0
surface	σ_{2min}	130	−46.6	−42.9	7.9
Bearing center E	Reaction F	N/A	126.3	125.8	0.4

Comparison of PFEM to MTMM

Table 4 shows the σ_{1max} and σ_{2min} results of the bend pulley obtained by using Qiu and Sethi's (1993) MTMM. Comparing the results in Table 4 with those in Table 2, the authors conclude that PFEM outperforms MTMM marginally. However, it is noted that at the cross section E (bearing location), the resultant reaction force calculated by MTMM is 5% lower than that of *ANSYS* while the resultant reaction force calculated by PFEM yields almost the same value as that of *ANSYS*. This is owing to the fact that PFEM preserve all modes of rigid body motions while MTMM only preserves two of six modes of rigid body motions.

Table 3. Case 2 Extreme Stresses (MPa) and Bearing Reaction Force (kN) by PFEM

Location	Stress type	θ (degrees)	*ANSYS*	PFEM	Error (%)
Cross section A inner	σ_{1max}	90	15.5	14.6	5.2
surface	σ_{2min}	20	−32.0	−30.9	3.4
Cross section B inner	σ_{1max}	355	41.0	42.3	3.3
surface	σ_{2min}	310	−15.4	−14.7	5.1
Cross section C inner	σ_{1max}	150	42.0	39.4	6.0
surface	σ_{2min}	315	−100.2	−83.8	16.4
Cross section D inner	σ_{1max}	275	64.5	63.8	1.1
surface	σ_{2min}	335	−50.9	−45.8	9.9
Bearing center E	Reaction F	N/A	825.4	823.5	0.2

Table 4. Case 1 Extreme Stresses (MPa) and Bearing Reaction Force (kN) by MTMM

Location	Stress type	θ (degrees)	*ANSYS*	MTMM	Error (%)
Cross section A inner	σ_{1max}	310	21.5	23.5	−9.5
surface	σ_{2min}	250	−28.7	−26.6	7.4
Cross section B inner	σ_{1max}	345	32.0	34.2	6.6
surface	σ_{2min}	0	−11.0	−8.5	22.5
Cross section C inner	σ_{1max}	355	40.1	41.6	3.6
surface	σ_{2min}	310	−43.0	−34.3	20.1
Cross section D inner	σ_{1max}	340	51.4	52.9	2.9
surface	σ_{2min}	130	−46.6	−42.1	9.8
Bearing center E	Reaction F	N/A	126.3	120.2	4.8

Conclusions

A rigorous and efficient precise finite-element model for conveyor pulley has been developed. Two examples of pulleys were chosen to validate PFEM models by comparison of the numerical solutions to *ANSYS* FEM solution. The numerical examples demonstrated the capabilities and the degree of accuracies of the model. The methodology may serve as a useful tool for designers of industrial pulleys.

References

ANSYS 10 [Computer software]. Canonsburg, PA, ANSYS.

Lange, H. (1963). "Investigations on stress in belt conveyor pulleys." Ph.D. thesis, Technical Univ. Hannover, Hannover, Germany.

Martins, J. A., and Kövesdy, I. (2012). "Overview in the application of FEM in mining and the study of case: Stress analysis in pulleys of stacker-reclaimers: FEM vs. analytical." Chapter 13, *Finite element analysis: Applications in mechanical engineering*, F. Ebrahimi, ed., InTech, Rijeka, Croatia, 277–296.

Patel, R. R., Joshi, S. P., and Agrawal, P. M. (2011). "Studies on some aspects of conveyor drive pulley design." *National Conf. on Recent Trends in Engineering & Technology*, BVM Engineering College, Anand, Gujarat, India.

Pathan, N. W., Bhope, D. V., and Khamankar, S. D. (2011). "Investigation of stresses in flat belt pulley by FEM and photoelasticity." *Int. J. Eng. Sci. Technol.*, 3(10), 7444–7451.

Qiu, X. (2006). "Full two-dimensional model for rolling resistance: Hard cylinder on viscoelastic foundation of finite thickness." *J. Eng. Mech.*, 10.1061/(ASCE)0733-9399(2006)132:11(1241), 1241–1251.

Qiu, X. (2009). "Full two-dimensional model for rolling resistance. II: Viscoelastic cylinders on rigid ground." *J. Eng. Mech.*, 10.1061/(ASCE)0733-9399(2009)135:1(20), 20–30.

Qiu, X., and Sethi, V. (1993). "A new pulley stress analysis method based on modified transfer matrix method." *J. Bulk Solids Handling*, 13(4), 713–724.
Ravikumar, M., and Chattopadhyay, A. (1999). "Integral analysis of conveyor pulley using finite element method." *Comp. Struct.*, 71(3), 303–332.
Sethi, V., and Nordell, L. K. (1993). "Modern pulley design techniques and failure analysis methods." *Proc., SME Annual Meeting & Exhibition*, Society for Mining, Metallurgy, and Exploration, Englewood, CO.
Timoshenko, S., and Woinowsky-Krieger, S. (1959). *Theory of plates and shells*, 2nd Ed., McGraw Hill, New York.
Ventsel, E., and Krauthammer, T. (2001). *Thin plates and shells theory, analysis, and applications*, Marcel Dekker, New York.
Vinogradov, A. M., and Kupershmidt, B. A. (1981). "The structures of Hamiltonian mechanics." *Integrable systems*, Cambridge University Press, London, 173–240.
Zhong, W. (1995). *A new systematic methodology for theory of elasticity*, Dalian University of Technology Press, Dalian, China.
Zhong, W., Zhu, J., and Zhong, X. (1996). "On a new time integration method for solving time dependent partial differential equations." *Comput. Methods Appl. Mech. Eng.*, 130(1–2), 163–178.